Measurement of Stress Redistribution in Flowing Emulsions

Kenneth W. Desmond and Eric R. Weeks
Department of Physics, Emory University, Atlanta, Georgia 30322, USA
(Received 31 May 2015; published 28 August 2015)

We study how local rearrangements alter droplet stresses within flowing dense quasi-two-dimensional emulsions at area fractions $\phi \geq 0.88$. Using microscopy, we measure droplet positions while simultaneously using their deformed shape to measure droplet stresses. We find that rearrangements alter nearby stresses in a quadrupolar pattern: stresses on neighboring droplets tend to either decrease or increase depending on location. The stress redistribution is more anisotropic with increasing ϕ. The spatial character of the stress redistribution influences where subsequent rearrangements occur. Our results provide direct quantitative support for rheological theories of dense amorphous materials that connect local rearrangements to changes in nearby stress.

DOI: 10.1103/PhysRevLett.115.098302 PACS numbers: 82.70.Kj, 47.50.Ef, 83.80.Iz

Soft glassy materials consist of particles that are disorderedly crowded together. Many of their physical properties depend on the control parameter ϕ, the fraction of volume occupied by particles. Such systems are glassy ("jammed") when ϕ exceeds a critical value ϕ_c such that the particles are forced into contact [1,2]. Under sufficient stresses, jammed systems will flow macroscopically via microscopic particle rearrangements [3,4]. These rearrangements result in stress and velocity fluctuations at the particle scale [1,5–9], and the size and frequency of these fluctuations are thought to relate to the macroscopic response of the material [10–12].

In such dense and disordered systems, simulations showed that particle rearrangements are initiated by a buildup of local interparticle stresses that become unstable. Particles rearrange and change the forces they exert on neighboring particles, leading to an anisotropic redistribution of stress over a few particle diameters [10–14]. This redistribution is of significant interest because it can increase the tendency for neighboring particles to undergo a rearrangement [10,11,15]. This can lead to avalanches, where one rearrangement alters the stress nearby and triggers a series of other rearrangements [11,16–18]. Such behavior implies that stress and strain rate are coupled nonlocally, and knowing the details of the stress redistribution is critical to accurately modeling soft glassy flows [15,17–19].

It is challenging to directly measure the stress redistribution over a large range of ϕ. Many prior experiments were limited to tracking particle positions without knowledge of the stresses [5–8,20–25]. Some simulations [10–13] focused on the dry foam limit $\phi \to 1$ where the gas bubbles occupy nearly all of the volume. Experiments with rigid or slightly deformable particles have the complementary limitation: because particles are close packed at ϕ_c, these experiments are done at $\phi \approx \phi_c$ [5,20–27]. No prior experiment has studied stresses over a large range of ϕ. In this Letter, we present experiments studying the flow of quasi-two-dimensional emulsion droplets over a large range of area fractions $\phi_c < \phi < 1$. We simultaneously measure droplet positions and interdroplet forces allowing us to quantify the connection between droplet rearrangements and stress redistribution.

We confine bidisperse emulsions (mineral oil in water) between two glass slides of dimensions 25×75 mm^2 separated by a $\sim$100 μm spacer (transparency film). We produce our droplets using microfluidics [28] and stabilize them from coalescence with Fairy soap [29]. Their diameters are larger than the sample chamber gap distance so that the system is quasi-2D. A schematic of our chamber is shown in Fig. 1, which consists of two channels of

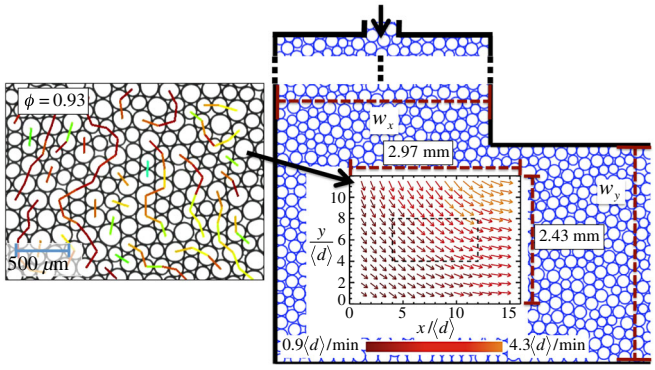

FIG. 1 (color online). Schematic of our two-dimensional flow geometry. The embedded flow field indicates the region where the flow is imaged (snapshot of this region shown on left with mean droplet diameter $\langle d \rangle = 188$ μm). The length and color of the arrows indicate mean velocity. The dashed black rectangle is the region in the field of view where $T1$ events are considered for analysis. On the snapshot, force chains [29] have been drawn as lines, where the largest forces are in red. Snapshot and velocity field both correspond to the first row of Table 1 in the Supplemental Material [30].

widths $w_x \approx w_y$ that meet at a right angle. A syringe pump injects the emulsion into the chamber, far upstream from the imaged region, as indicated in Fig. 1. In the corner, droplets change direction, resulting in many rearrangements. We take a total of 13 data sets at different area fractions ϕ ranging between 0.88 and 0.96 and at 4 different strain rates, $\dot{\gamma} = 1.3$–$5.5\ \mathrm{h}^{-1}$ (see Table 1 in Supplemental Material for experimental details [30]). We record images with a CCD camera at 2 images/s. We postprocess the images to identify [29] and track droplets [31].

Figure 1 shows a typical flow field in the region where we take our data. There is a velocity gradient that induces droplet rearrangements. The gradient is nonuniform, giving a strain rate that depends on space, although it varies by no more than a factor of ~2 across the field of view for our experiments. For the strain rates we study, our results are independent of strain rate. Accordingly, from the droplet trajectories we determine the global (mean) strain rate within our observation region and report this as $\dot{\gamma}_{\mathrm{global}}$ for each data set presented in Table 1 of the Supplemental Material [30].

We also determine the repulsive contact force $\vec{f}_{ij}$ between droplets i and j in contact. The quasi-2D droplets prefer to have circular outlines due to surface tension, and their deformation away from circular can be related to the contact forces within 15% uncertainty using our previously developed image analysis technique [29]. Figure 1 shows some of the larger forces between droplets. We also determine the viscous droplet-droplet forces (less than 1% of the mean repulsive force) and droplet-glass forces (less than 4% of the mean repulsive force); see Ref. [32] for details. Since the viscous forces are small, we ignore their contribution to the stress.

Using the repulsive contact forces, the instantaneous stress tensor on each droplet is computed using

$$\overleftrightarrow{\sigma}_i = 1/A_i \sum_j \vec{r}^{\,c}_{ij} \otimes \vec{f}_{ij}, \qquad (1)$$

where $\vec{r}^{\,c}_{ij}$ is a vector from the center of droplet i to the center of contact ij, $\otimes$ is an outer product, and A_i is the Voronoi area around droplet i [33,34]. The off-diagonal term of this tensor is the shear stress, which depends on the orientation of the coordinate system. We rotate the coordinate system to maximize the time- and droplet-averaged off-diagonal term of the stress tensor; this rotation is ≈45° (but varies slightly from experiment to experiment). In this rotated coordinate system, we use the instantaneous off-diagonal element as the instantaneous shear stress $\sigma_i(t)$ on each droplet.

In 2D systems, the simplest topological rearrangements involve neighbor exchanges of four droplets [35], known as a $T1$ event. This exchange is shown in Fig. 2(a): two neighboring droplets become next-nearest neighbors while two next-nearest neighbors become neighbors. Sometimes

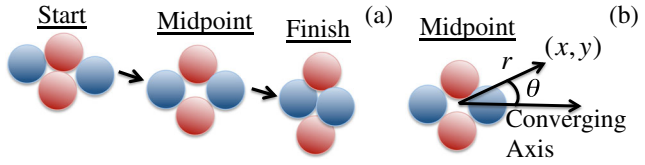

FIG. 2 (color online). (a) $T1$ event, where 4 droplets exchange neighbors. (b) Coordinate system relative to midpoint of $T1$ event. The converging axis is the line joining the centers of the two droplets moving closer together; the direction of the axis is arbitrary. This axis defines the Cartesian coordinates (x, y) and polar coordinates (r, θ).

larger groups of droplets rearrange simultaneously, but such events can always be decomposed into individual $T1$ events [9]. To define the start and end of a $T1$ event, we consider only $T1$ events that lead to a stress relaxation on the four rearranging droplets, and define the start as the time where the stress is maximal before the neighbor exchange and the end as the minimum in stress after the neighbor exchange. Between the start and the end of the $T1$ event the stress decreases by $\delta\sigma_{T1}$, which varies between rearrangements.

To examine the variability of $\delta\sigma_{T1}$, we show the probability distributions of $\delta\sigma_{T1}$ as the curves in Fig. 3. After normalizing by the mean stress drop $\langle\delta\sigma_{T1}\rangle$, all distributions overlap. Intriguingly, the distributions resemble the distribution of the instantaneous individual droplet stresses $P(\sigma_i/\langle\sigma\rangle)$, plotted as triangles in Fig. 3 (at a representative area fraction $\phi = 0.93$; the shape does not vary significantly at different ϕ).

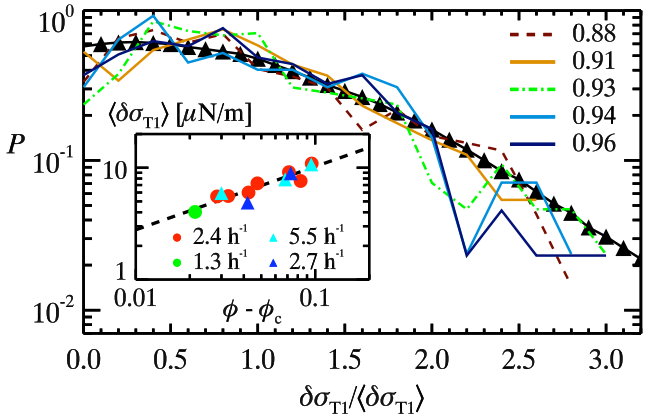

FIG. 3 (color online). Distribution of stress decrease on the rearranging droplets. The color of the curve indicates area fraction. The solid curves are data at $\dot{\gamma} = 5.5\ \mathrm{h}^{-1}$, the dashed lines at $\dot{\gamma} = 2.7\ \mathrm{h}^{-1}$, and the dash-dotted lines at $\dot{\gamma} = 2.4\ \mathrm{h}^{-1}$. The filled triangle black curve is the distribution of individual droplet shear stresses σ_i in a sample at $\phi = 0.89$, normalized by $\langle\sigma_i\rangle$. Inset: Average stress relaxation with area fraction. The legend indicates data at different strain rates. The black dashed line is a power-law fit $\langle\delta\sigma\rangle = A(\phi - \phi_c)^{\beta}$, where $\beta = 0.57$, $A = 38\ \mu\mathrm{N/m}$, and $\phi_c = 0.86$.

While the variation in $\delta\sigma$ about the mean is independent of the area fraction, the mean stress drop is not. In the inset of Fig. 3, we show that $\langle\delta\sigma\rangle$ increases with area fraction relative to the jamming point $\phi_c = 0.86$, where ϕ_c was measured in Ref. [29]. The data for different strain rates overlap, as we are in the rate-independent regime. We fit the data using $\langle\delta\sigma\rangle \sim (\phi - \phi_c)^\beta$ with $\beta = 0.57$, similar to scaling behavior found for the shear modulus, pressure, and coordination number [1,36].

Thus far we have focused on the stress drop averaged over the four droplets defining the $T1$ event. We next examine how the $T1$ event redistributes stress on the rest of the sample. To do this, we define a coordinate system for each $T1$ event, as shown in Fig. 2(b), using the converging direction of droplets as the x axis. Positions are measured relative to the center of the $T1$ event.

The stress redistribution around a $T1$ event can be characterized by a stress propagator $\Pi(x, y)$, defined as $\delta\sigma(x, y) = \Pi(x, y)\delta\sigma_{T1}$. Here, $\delta\sigma(x, y)$ is the change in stress on a droplet located a distance (x, y) away from a $T1$ event that has a particular stress drop of size $\delta\sigma_{T1}$. Given a stress fluctuation on the rearranging droplets, $\Pi(x, y)$ quantifies the mean size of the stress fluctuation at (x, y). Recall that $\delta\sigma_{T1}$ measures the amount the stress has decreased, and thus, when $\Pi(x, y)$ is positive, the stress at (x, y) decreased. We will focus on the stress propagator $\Pi(x, y)$ averaged over 100–600 $T1$ events (we ignore the angular brackets in our notation).

Figure 4 shows the measured stress propagator for a range of area fractions. The stress can decrease (positive Π, blue) or increase (negative Π, orange) on nearby droplets depending on their relative position to the $T1$ event. Along the converging and diverging axes we find that for all ϕ the stress decreases on droplets near the rearrangement. In contrast, along the directions 45° to the converging and diverging directions, the stress change depends on ϕ. At low area fractions, the stress propagators show that a rearrangement tends to decrease the stress on all nearby droplets, while at larger area fractions, droplets along the diagonal directions tend to have their stress increased.

Picard *et al.* [13] model a $T1$ event as a localized region undergoing pure shear within a continuous elastic material. They predict a quadrupolar field for the stress propagator obeying $\Pi = (\langle d\rangle/r)^2 \cos(4\theta)$, similar in form to that derived by Eshelby for an analogous inclusion problem [37,38], and shown in the bottom right-hand panel of Fig. 4. In simulations on dry foams ($\phi = 1$), Kabla and Debrégeas [12] observed a qualitatively similar quadrupolar stress propagator, and this was subsequently seen in a simulation of a 2D glass [14].

We test the prediction of Picard *et al.* of a $1/r^2$ scaling by looking at Π along the converging and diverging directions. An example is given in Fig. 5(a). The data are consistent with $1/r^2$ decay, indicated by the dotted line. Next we

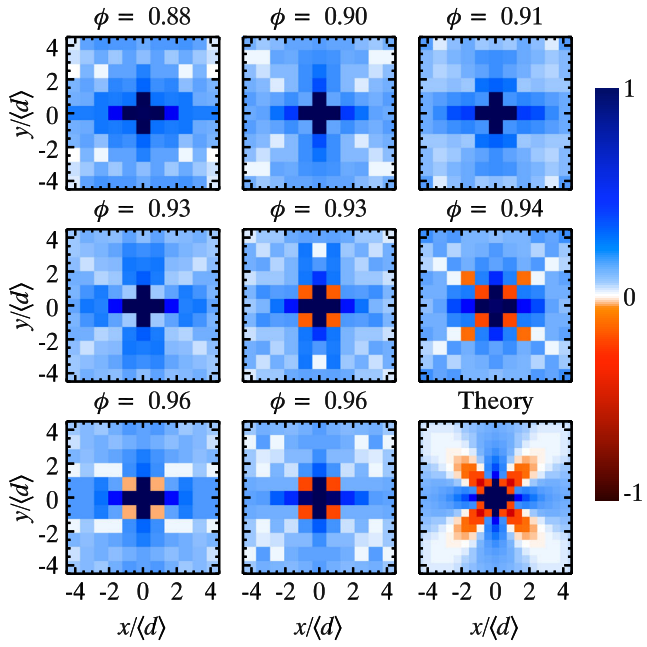

FIG. 4 (color online). Measured stress propagators. The last panel is the theoretical stress propagator for $\phi = 1$ [13]. Blue indicates an average stress decrease and red indicates a stress increase. Distance to center of $T1$ event is measured in units of average droplet diameters. Both $\phi = 0.93$ panels and both $\phi = 0.96$ panels are two different samples with the same ϕ, indicating that the stress propagator is not completely reproducible between experiments. To improve statistics in each panel, we impose fourfold symmetry on Π. Prior to imposing symmetry, the raw data have fourfold symmetry within the statistical noise limit.

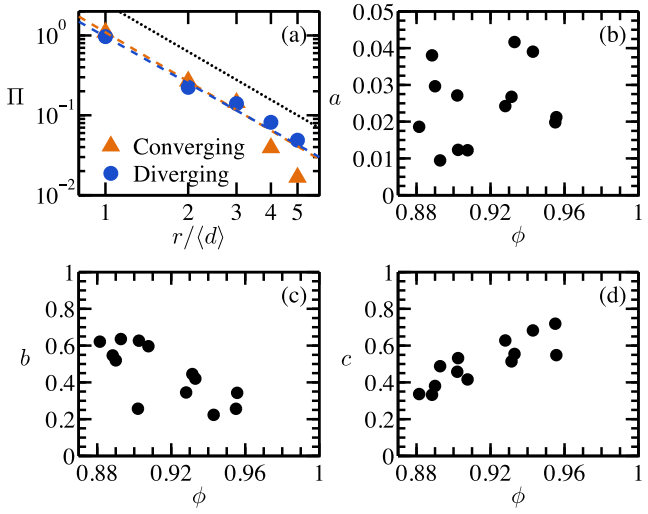

FIG. 5 (color online). (a) Decay of stress propagator along the converging and diverging directions in a sample at $\phi = 0.89$. The colored dashed lines are power-law fits $\Pi \sim r^{-\alpha}$, with $\alpha = 2.04$ and 1.94 for the converging and diverging directions, respectively. For comparison, the black dotted line has power-law slope −2. (b)–(d) The stress propagator for each data set is fit to $\Pi_{\text{model}} = a + b(\langle d\rangle/r)^2 + c(\langle d\rangle/r)^2 \cos(4\theta)$, and the fitting parameters a, b, and c are shown as functions of area fraction.

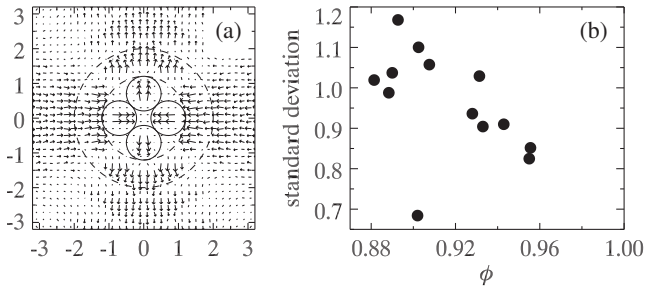

FIG. 6. (a) Mean displacement $\vec{u}_{\mathrm{av}}(x,y)$ of droplets near a $T1$ event—four circles are the mean positions of droplets undergoing a $T1$ event and the axes are in units of $\langle d\rangle$. The mean displacement field does not vary with ϕ, so data are averaged from all experiments, and fourfold symmetry is imposed. (b) We compute the standard deviation at each (x,y) between the mean flow field $\vec{u}_{\mathrm{av}}(x,y)$ and the flow fields $\vec{u}_i(x,y)$ around each $T1$ event i. The standard deviation is spatially averaged within a ring of radius $1.2\langle D\rangle \le R \le 2.0\langle D\rangle$ around the $T1$ event centers [dashed circles in (a)] and is plotted in (b) as a function of area fraction. $\vec{u}_i(x,y)$ is normalized by the mean displacement of the $T1$ droplets for each ϕ, so a value of 1 in the standard deviation means that the variability of droplet displacements is equal to the magnitude of the displacement of the $T1$ droplets.

quantify the anisotropy of the stress propagator by adding onto the prediction of Picard *et al.* two isotropic terms, and fitting the raw data (without imposing fourfold symmetry) to $\Pi_{\mathrm{model}} = a + b(\langle d\rangle/r)^2 + c(\langle d\rangle/r)^2\cos(4\theta)$, with fit parameters a, b, and c. This is an empirical fit that works well for all our data.

The fitting parameters are shown in Figs. 5(b)–5(d). The monopole term a has no apparent ϕ dependence, and is slightly positive, indicating that the global stress tends to decrease during a $T1$ event. b (the isotropic term) decreases with ϕ, while c (the quadrupolar anisotropic term) increases with ϕ. These trends indicate a transition from an anisotropic stress relaxation to an isotropic one as the jamming area fraction ($\phi_c = 0.86$) is approached from above. This may be due to a change in the nature of how droplets move relative to each other as ϕ_c is approached. Near ϕ_c, droplets contact an average of four neighboring droplets, while as $\phi \to 1$, droplets contact all of their neighbors, six on average [1,2]. The latter situation is closest to the isotropic homogeneous elastic materials that Picard *et al.* considered [13] (and earlier Eshelby [37,38]). In contrast, near ϕ_c, exactly how neighboring droplets move varies between different $T1$ events.

Figure 6 confirms that as the jamming point is approached from above, the motion of droplets near a $T1$ event is more variable. Figure 6(a) shows the mean displacement field around a $T1$ event, with a dipole structure as expected and as seen in prior work [14,22,25,39]. Figure 6(b) plots the variability in the displacement field between $T1$ events, demonstrating that droplets exhibit larger fluctuations from the mean as $\phi \to \phi_c$ from above. (The outlier at $\phi = 0.90$ is for the experiment with the fewest number of $T1$ events, 111, although we do not see any other discrepant behavior for this experiment.) The variable flow fields at low ϕ suggest that the stress redistribution pattern will also be more variable from event to event, thus leading to a more isotropic Π when the data are averaged.

Our experiments demonstrate that simple rearrangement events ($T1$ events) relax the stress on neighboring droplets. At higher area fractions, this stress relaxation has a quadrupolar character, confirming theoretical predictions [13]. One implication is that T1 events increase the stress felt by nearby droplets along certain directions, and subsequent $T1$ events are more likely to occur in those regions. This is indeed true in our experiments (data not shown). Because of a change in the character of particle motion at lower area fractions, the stress redistribution becomes less quadrupolar and more isotropic as the jamming point ϕ_c is approached from above. This reflects the spatial heterogeneity in these systems as $\phi \to \phi_c$ [2]. Our observations provide direct evidence that on a droplet scale rearrangements in one location influence stresses felt in other locations, and that the area fraction determines the details of how this influence is propagated.

This work was supported by the National Science Foundation (Grants No. CBET-0853837 and No. CBET-1336401).

[1] D. J. Durian, Phys. Rev. Lett. **75**, 4780 (1995).
[2] A. J. Liu and S. R. Nagel, Annu. Rev. Condens. Matter Phys. **1**, 347 (2010).
[3] T. G. Mason, J. Bibette, and D. A. Weitz, J. Colloid Interface Sci. **179**, 439 (1996).
[4] T. G. Mason, Curr. Opin. Colloid Interface Sci. **4**, 231 (1999).
[5] B. Miller, C. O'Hern, and R. P. Behringer, Phys. Rev. Lett. **77**, 3110 (1996).
[6] S. Tewari, D. Schiemann, D. J. Durian, C. M. Knobler, S. A. Langer, and A. J. Liu, Phys. Rev. E **60**, 4385 (1999).
[7] M. Dennin, Phys. Rev. E **70**, 041406 (2004).
[8] J. Lauridsen, G. Chanan, and M. Dennin, Phys. Rev. Lett. **93**, 018303 (2004).
[9] D. Chen, K. W. Desmond, and E. R. Weeks, Soft Matter **8**, 10486 (2012).
[10] G. Picard, A. Ajdari, F. Lequeux, and L. Bocquet, Phys. Rev. E **71**, 010501 (2005).
[11] A. Kabla, J. Scheibert, and G. Debregeas, J. Fluid Mech. **587**, 45 (2007).
[12] A. Kabla and G. Debrégeas, Phys. Rev. Lett. **90**, 258303 (2003).
[13] G. Picard, A. Ajdari, F. Lequeux, and L. Bocquet, Eur. Phys. J. E **15**, 371 (2004).
[14] A. Tanguy, F. Leonforte, and J. L. Barrat, Eur. Phys. J. E **20**, 355 (2006).
[15] J. Goyon, A. Colin, G. Ovarlez, A. Ajdari, and L. Bocquet, Nature (London) **454**, 84 (2008).

[16] G. Debrégeas, H. Tabuteau, and J. M. di Meglio, Phys. Rev. Lett. **87**, 178305 (2001).
[17] O. Pouliquen and Y. Forterre, Phil. Trans. R. Soc. A **367**, 5091 (2009).
[18] K. Kamrin and G. Koval, Phys. Rev. Lett. **108**, 178301 (2012).
[19] L. Bocquet, A. Colin, and A. Ajdari, Phys. Rev. Lett. **103**, 036001 (2009).
[20] R. Besseling, E. R. Weeks, A. B. Schofield, and W. C. K. Poon, Phys. Rev. Lett. **99**, 028301 (2007).
[21] D. Chen, D. Semwogerere, J. Sato, V. Breedveld, and E. R. Weeks, Phys. Rev. E **81**, 011403 (2010).
[22] V. Chikkadi, G. Wegdam, D. Bonn, B. Nienhuis, and P. Schall, Phys. Rev. Lett. **107**, 198303 (2011).
[23] J. A. Dijksman, F. Rietz, K. A. Lőrincz, M. van Hecke, and W. Losert, Rev. Sci. Instrum. **83**, 011301 (2012).
[24] A. Le Bouil, A. Amon, S. McNamara, and J. Crassous, Phys. Rev. Lett. **112**, 246001 (2014).
[25] K. E. Jensen, D. A. Weitz, and F. Spaepen, Phys. Rev. E **90**, 042305 (2014).
[26] B. Utter and R. P. Behringer, Phys. Rev. Lett. **100**, 208302 (2008).
[27] D. Howell, R. P. Behringer, and C. Veje, Phys. Rev. Lett. **82**, 5241 (1999).
[28] R. Shah, H. Shum, A. Rowat, D. Lee, J. Agresti, A. Utada, L. Chu, J. Kim, A. Fernandez-Nieves, and C. Martinez, Mater. Today **11**, 18 (2008).
[29] K. W. Desmond, P. J. Young, D. Chen, and E. R. Weeks, Soft Matter **9**, 3424 (2013).
[30] See Supplemental Material at http://link.aps.org/supplemental/10.1103/PhysRevLett.115.098302 for table of experimental parameters.
[31] J. C. Crocker and D. G. Grier, J. Colloid Interface Sci. **179**, 298 (1996).
[32] K. W. Desmond, Ph.D. thesis, Emory University, 2012, https://vmch-etd.library.emory.edu/view/record/pid/emory:bnwwx.
[33] F. da Cruz, S. Emam, M. Prochnow, J. N. Roux, and F. Chevoir, Phys. Rev. E **72**, 021309 (2005).
[34] M. P. Allen and D. J. Tildesley, *Computer Simulation of Liquids* (Oxford University Press, New York, 1989).
[35] M. Lundberg, K. Krishan, N. Xu, C. S. O'Hern, and M. Dennin, Phys. Rev. E **77**, 041505 (2008).
[36] D. J. Durian, Phys. Rev. E **55**, 1739 (1997).
[37] J. D. Eshelby, Proc. R. Soc. A **241**, 376 (1957).
[38] J. D. Eshelby, Proc. R. Soc. A **252**, 561 (1959).
[39] W. G. Ellenbroek, E. Somfai, M. van Hecke, and W. van Saarloos, Phys. Rev. Lett. **97**, 258001 (2006).